



Published in final edited form as:

Mucosal Immunol. 2016 July ; 9(4): 1065–1075. doi:10.1038/mi.2015.124.

A STING-dependent innate sensing pathway mediates resistance to corneal HSV-1 infection via upregulation of the antiviral effector tetherin

D.J. Royer and D.J.J. Carr^{1,2}

¹Department of Microbiology & Immunology, The University of Oklahoma Health Sciences Center, Oklahoma City, OK USA.

²Department of Ophthalmology, The University of Oklahoma Health Sciences Center, Oklahoma City, OK USA.

Abstract

Type 1 interferons (IFN α/β) mediate immunologic host resistance to numerous viral infections including herpes simplex virus type 1 (HSV-1). The pathways responsible for IFN α/β signaling during the innate immune response to acute HSV-1 infection in the cornea are incompletely understood. Using a murine ocular infection model, we hypothesized that the stimulator of IFN genes (STING) mediates resistance to HSV-1 infection at the ocular surface and preserves the structural integrity of this mucosal site. Viral pathogenesis, tissue pathology, and host immune responses during ocular HSV-1 infection were characterized by plaque assay, esthesiometry, pachymetry, immunohistochemistry, flow cytometry, and siRNA transfection in wildtype C57BL/6 (WT), STING-deficient (STING^{-/-}), and IFN α/β receptor-deficient (CD118^{-/-}) mice at days 3–5 post infection. The presence of STING was critical for sustained control of HSV-1 replication in the corneal epithelium and neuroinvasion, but loss of STING had a negligible impact with respect to gross tissue pathology. Auxiliary STING-independent IFN α/β signaling pathways were responsible for maintenance of the corneal integrity. Lymphatic vessels, mast cells, and sensory innervation were compromised in CD118^{-/-} mice concurrent with increased tissue edema. STING-dependent signaling led to the upregulation of tetherin, a viral restriction factor we identify is important in containing the spread of HSV-1 *in vivo*.

INTRODUCTION

Viral infections set off cellular alarms through the detection of pathogen-associated molecular patterns (PAMPs). Virus-derived PAMPs are recognized by a variety of innate sensors that operate through distinct signaling pathways to upregulate IFN α/β and stimulate NF- κ B-driven cytokine production.¹ IFN α/β secretion mediates canonical autocrine and paracrine signaling through the IFN α/β receptor (CD118). The IFN α/β signaling pathway

Corresponding Author: Daniel J.J. Carr, Address: Department of Ophthalmology, DMEI Acers Pavilion, Room 415, 608 Stanton L. Young Blvd., Oklahoma City, OK 73104, Phone: 405-271-8784, Dan-Carr@ouhsc.edu.

Disclosure: the authors have no financial or commercial conflicts of interest

Online supplemental material. Supplementary data is available online at www.nature.com/mi

modulates hundreds of IFN-stimulated genes (ISGs), the products of which activate immunologic countermeasures and promote host resistance to viral infections.² Specific host-pathogen interactions ultimately dictate the effectiveness of IFN α/β signaling, as many viruses including HSV-1 employ numerous mechanisms to evade, counteract, or otherwise disrupt pathway components or downstream ISGs.^{3,4}

Multiple pattern recognition receptor families can initiate IFN α/β signaling during DNA virus infections.⁵⁻⁷ The pathways by which HSV-1-derived PAMPs mediate IFN α/β induction and host resistance within mucosal sites are incompletely understood. Our lab has previously shown that loss of toll-like receptor (TLR) signaling does not enhance HSV-1 pathogenesis in the cornea; rather, a TLR-independent pathway involving the STING-dependent DNA sensor IFI16 (IFN inducible protein 16) initiates host resistance to HSV-1 in the corneal epithelium.⁸ STING operates as a direct sensor of cytosolic DNA and a central signaling adaptor protein for an array of cytoplasmic and nuclear DNA sensors.^{6,9} STING-dependent induction of IFN α/β involves activation of the transcription factor IFN regulatory factor 3 (IRF3) via phosphorylation by TANK-binding kinase 1 (TBK1).¹⁰ IFI16 has been linked to early IFN β production in HSV-1-infected monocyte/macrophage cell lines, fibroblasts, and in the corneal epithelium.^{8,11,12} However, IFI16 is degraded by the HSV-1 early gene product ICP0, suggesting that the STING-TBK1-IRF3 signaling axis is essential for early detection of viral infection but may be subsequently counteracted by the virus.^{11,13,14} We investigated the role of STING in sustained IFN α/β signaling in a mouse model of ocular HSV-1 infection, and hypothesized that STING mediates innate host resistance to corneal HSV-1 infection and preserves the corneal integrity through day 5 pi.

Currently, there are no prophylactic or therapeutic vaccines licensed to prevent sequelae elicited by HSV-1 infection.¹⁵ These medically relevant pathologies span in severity from intermittent mucocutaneous lesions (*i.e.* oral and genital herpes, herpetic keratitis) to neurological damage and corneal blindness.¹⁶ The cornea is a delicate mucosal site, and pathological alteration of the tissue architecture hinders visual acuity. Recurrent corneal HSV-1 infection contributes to a variety of pathological sequelae in the human cornea that can affect visual acuity and health of the ocular surface including edema, scarring, neovascularization, and loss of sensation.^{15,17} Our investigation highlights the subtleties of IFN α/β -signaling pathways in promoting resistance to ocular HSV-1 infection. Resistance to HSV-1 involves the coordinated activities and interactions of many cell types and structures in the cornea to detect the viral infection, limit local replication, and impede spread to peripheral nerve ganglia. Our findings collectively identify that the STING signaling axis is critical for host resistance to corneal HSV-1 infection through a mechanism involving the viral restriction factor tetherin (also known as BST2, CD317, HM1.24, PDCA-1). A wealth of evidence supports tetherin as a viral restriction factor active against a diverse range of enveloped viruses *in vitro* and *in vivo* by impeding cell-cell spread of nascent virions.¹⁸⁻²⁰ We show that tetherin limits HSV-1 replication in the corneal epithelium and impedes viral dissemination to the nervous system.

RESULTS

STING promotes sustained resistance to HSV-1 replication in the eye

To identify the impact of STING relative to acute HSV-1 infection of the ocular surface, HSV-1 infection of the cornea was modeled using wild type (WT) C57BL6/J, STING-deficient (STING^{-/-}), and highly susceptible IFN α / β receptor-deficient (CD118^{-/-}) mice. By day 5 post infection (pi), STING^{-/-} and CD118^{-/-} mice harbored significantly more infectious virus in the cornea than WT mice (Figure 1a). A moderate increase in titer comparing CD118^{-/-} mice to STING^{-/-} mice was also observed (Figure 1a). This data indicates that the STING-signaling pathway is a major determinant of IFN α / β -dependent host resistance within the cornea following HSV-1 infection.

STING deficiency does not exacerbate acute corneal pathology

Corneal sensation and edema were measured following HSV-1 infection via Cochet-Bonnet esthesiometry and ultrasound pachymetry, respectively. WT mice had no appreciable changes in corneal sensation (Figure 1b) relative to healthy controls (not shown) by day 5 pi, though significant sensation loss and corneal denervation is observed in WT mice by day 8 pi using this experimental model.²¹ In contrast, CD118^{-/-} mice exhibited hyperacute corneal sensation loss such that the pressure required to elicit a blink response was 15 g/mm² higher than WT by day 5 pi (Figure 1b).

Despite the similar magnitude of infectious virus recovered from the corneas of STING^{-/-} and CD118^{-/-} mice, corneal sensation loss relative to WT was not observed in STING^{-/-} mice through day 5 pi (Figure 1b). Corneas of CD118^{-/-} mice were more edematous than either STING^{-/-} or WT mice by day 3 pi (Figure 1c). The severity of corneal edema continued to worsen in CD118^{-/-} mice through day 5 pi, while differences in corneal thickness observed in WT and STING^{-/-} mice following infection were generally unremarkable compared to baseline uninfected (UI) controls (Figure 1c). Moreover, the mechanism underlying HSV-1 associated corneal sensation loss is likely dependent on intrinsic cell-signaling pathways and is not merely attributable to infection of the sensory neurons, as STING^{-/-} and CD118^{-/-} mice harbored 100–1000 times more infectious virus in the TG than WT by day 5 pi (data not shown; $p < 0.001$).

STING promotes host resistance in the corneal epithelium and restrains HSV-1 neuroinvasion

Confocal imaging was employed to visualize the localization of HSV-1 antigen in cornea whole mounts at day 5 pi. Viral lesions were geographically isolated in WT corneas, whereas diffuse HSV-1 labeling was observed in STING^{-/-} and CD118^{-/-} corneas (Figure 1d). High-magnification confocal analysis of the viral lesions revealed that HSV-1 antigen is present almost exclusively in the outermost epithelial layers of WT and STING^{-/-} corneas but penetrates into the deeper stromal layers of CD118^{-/-} corneas (Figure 1e).

The pathogenesis of HSV-1 involves neuroinvasion and retrograde dissemination to the tissue-innervating trigeminal ganglion (TG) following infection of the oculo-oro-facial mucosae. Subbasal sensory nerve fibers of TG neurons innervate the corneal epithelium and

enable direct epithelial-nerve spread of HSV-1. CD118^{-/-} and STING^{-/-} mice harbored 100 times more infectious HSV-1 in the TG than WT as early as day 3 pi (Supplemental Figure 1a), indicating that STING-mediated signaling restricts dissemination of HSV-1 from the corneal epithelium to the nervous system.

STING deficiency leads to a minimal reduction in ISG expression

We hypothesized that the STING signaling axis drives and sustains IFN α/β production in the cornea following HSV-1 infection. To investigate this hypothesis, a modest gene array was utilized to measure downstream ISGs at day 5 pi. Cluster image mapping (Figure 2a) and quantification (Figure 2b) of compiled data show comparatively similar profiles for WT and STING^{-/-} mice and a paucity of transcript expression in CD118^{-/-} mice with respect to genes upregulated by IFN α/β -signaling. Still, other genes are repressed by IFN α/β signaling²² such as Wars, which exhibits higher expression in the CD118^{-/-} group than in WT or STING^{-/-} samples (Figure 2b).

Statistical analysis divulged a reduction in transcript expression comparing STING^{-/-} to WT mice for Bst2, Irf3, Irf9, Oas2, Oas3, and Rnasel (Figure 2b). Of these, the viral restriction factor Bst2 (tetherin) was the only transcript identified with pronounced margins of differential expression. Tetherin was highly upregulated in WT corneas yet expression was nearly 10 times lower in STING^{-/-} and CD118^{-/-} corneas (Figure 2b), consistent with the observed differences in viral pathogenesis in our model (Figure 1a). Despite being statistically significant, expression differences in the other genes of interest were less impressive and not pursued minor and not predicted to evoke meaningful physiological changes.

Amplified myeloid cell recruitment is observed in STING deficient mice

To uncover the immunologic mechanisms responsible for STING-dependent resistance to HSV-1 in the cornea, infiltrating leukocytes and cytokine concentrations were investigated. Flow cytometry was used to evaluate and characterize the cornea-infiltrating myeloid cells at day 5 pi. STING^{-/-} mice had nearly twice as many total infiltrating myeloid cells (CD45⁺ CD11b⁺) as WT mice (Figure 3a). Confocal microscopy used to confirm uniform distribution of CD11b⁺ cells throughout cornea flat mounts at day 5 pi for all three genotypes (data not shown). WT and CD118^{-/-} mice had comparable total numbers of infiltrating myeloid cells (Figure 3a). Ly6C and Ly6G antigens were used to distinguish monocytes and neutrophils (PMN). No statistical difference was measured in the total number of cornea-infiltrating Ly6C^{low} Ly6G^{hi} PMN comparing WT, STING^{-/-}, and CD118^{-/-} mice, although there was a propensity for the proportion of PMN to be elevated in CD118^{-/-} mice (Figure 3b).

Differences were observed in Ly6C⁺ cornea-infiltrating monocytes at day 5 pi. We identified two distinct Ly6C⁺ (mid-high) monocyte populations comprising Ly6G^{high} (Figure 3c) and Ly6G^{low} (Figure 3d) subsets. The ratio of the Ly6G^{high} to Ly6G^{low} monocyte subsets was also evaluated (Figure 3e). The Ly6C⁺ Ly6G^{low} monocyte population is largely absent in the corneas of CD118^{-/-} mice (Figure 3d) consistent with their identity as inflammatory monocytes, which serve as innate sentinels against HSV-1.²³ Representative dot plots are

shown for WT, STING, and CD118^{-/-} mice (Figure 3f). A higher ratio of Ly6C⁺ Ly6G^{high} monocytes was observed in the CD118^{-/-} corneas compared to STING^{-/-} or WT groups (Figure 3e), and a higher total number of Ly6C⁺ Ly6G^{high} monocytes were present in the corneas of STING^{-/-} mice than in other groups.

Despite the high number of inflammatory monocytes (Ly6C⁺ Ly6G^{low}) recruited into the corneas of STING^{-/-} mice, HSV-1 replication in the epithelium is not controlled (Figure 1a,e). However, gross tissue edema (Figure 1c) and viral penetration into the stroma (Figure 1e) are prevented in STING^{-/-} mice, which we attribute in part to the antiviral effects of inflammatory monocyte infiltration. Protein concentrations of IFN $\alpha_{2,4}$ and IFN γ in STING^{-/-} corneas were comparable to or exceeded WT at day 5 pi (Figure 3g), thus substantiating the ISG array findings (Figure 2). No elevation in IFN $\alpha_{2,4}$ concentrations were observed in WT or STING^{-/-} corneas relative to UI at day 3 pi (not shown). Concentrations of the monocyte chemotactic C-C motif chemokine ligands CCL2 and CCL20 were elevated in STING^{-/-} corneas at day 5 pi (Figure 3h), thus providing a mechanistic explanation for the observed enhancement in monocyte infiltration.^{23,24} Production of the proinflammatory cytokines IL-1 β and IL-17 were also measured (Figure 3i), but the concentrations detected did not correlate with severity of tissue pathology or viral pathogenesis.

In order to rule out a potential functional defect in the inflammatory monocytes in STING^{-/-} mice, CD11b⁺ splenocytes were isolated from uninfected WT or STING^{-/-} mice and inoculated *in vitro* with HSV-1 at various multiplicities of infection (MOI). Supernatant virus titers did not differ between WT and STING^{-/-} CD11b⁺ splenocyte cultures observed at 24 hours pi (Supplemental Figure 2a). By 48 hours pi, similar findings were observed in culture supernatants with a subtle variance at 1 MOI in which there was a modest but statistically significant increase in HSV-1 recovered from the infected CD11b⁺ STING^{-/-} cell cultures (Figure 3j). Prior to isolation of CD11b⁺ cells, splenocytes isolated from healthy WT and STING^{-/-} mice had a similar distribution of CD45⁺ CD11b⁺ myeloid cell subsets based on Ly6C and F4/80 antigen expression (Supplemental Figure 2b). CD11b⁺ splenocytes cultured for 24 hours showed no differences in the relative proportions of F4/80⁺ Ly6C⁻ macrophages or F4/80⁺ Ly6C^{mid-high} monocytes in the presence or absence of HSV-1 (Supplemental Figure 2c,d). Consistent with previous findings,²⁵ macrophages isolated from STING^{-/-} mice exhibited a deficit in major histocompatibility class II (MHC II) upregulation relative to WT in HSV-1 infected cultures (Supplemental Figure 2d). However, MHC II expression profiles were similar in both WT and STING^{-/-} monocyte subsets (Supplemental Figure 2c,d), thereby providing no phenotypic indication of functional defects in STING^{-/-} monocytes.

Peri-corneal lymphatic vessels and mast cells are lost in CD118^{-/-} mice

Corneal neovascularization and/or impairment of the peri-corneal vasculature were examined to further characterize differences in acute ocular pathology following HSV-1 infection. Blood and lymphatic vessels were labeled using anti-CD31 and anti-Lyve-1 antibodies, respectively, to visualize the peri-corneal vasculature at day 5 pi (Figure 4a). The vasculature of STING^{-/-} mice resembled WT (Figure 4a). Neovascularization was modest in

the WT and STING^{-/-} mice and notably absent in the CD118^{-/-} animals by day 5 pi (Figure 4a) relative to healthy UI corneas (not shown). The peri-corneal blood vessels remaining in CD118^{-/-} mice were distended relative to those seen in STING^{-/-} or WT mice (Figure 4a) consistent with observations of enhanced tissue edema in CD118^{-/-} mice (Figure 1c). Moreover, a profound loss of the lymphatic vasculature is observed in CD118^{-/-} mice by day 5 pi (Figure 4a).²⁶

Tissue-resident mast cells associated with the peri-corneal vasculature were also investigated at day 5 pi due to their pleiotropic immunomodulatory capacity²⁷ and protective role against ocular HSV-1 infection.²⁸ Mast cells were identified by avidin staining and found in the limbal aspect of the corneas of WT and STING^{-/-} mice as previously described.²⁸ In stark contrast, mast cells were lost in the corneas of CD118^{-/-} mice by day 5 pi (Figure 4b). We speculate the pathological corneal edema observed in CD118^{-/-} mice results from multiple mechanisms including: penetration of HSV-1 into the stroma, lymphatic vessel destruction, and loss of mast cells.

STING is required for tetherin expression in the corneal epithelium

A direct STING-dependent mechanism responsible for containment of viral replication and dissemination remained to be identified. Due to its expression profile in the ISG array, the viral restriction factor tetherin (also known as BST2, CD317, HM1.24, PDCA-1) was explored as a candidate in controlling HSV-1 in the corneal epithelium. We hypothesized that tetherin impedes spread of HSV-1 in the cornea in a STING-dependent manner. Immunolabeling in WT, STING^{-/-}, and CD118^{-/-} corneas at day 5 pi was utilized to identify the presence and localization of tetherin (Figure 4c). Tetherin colocalized with the CD31⁺ blood vessels in all groups. In contrast, high levels of tetherin protein expression was observed in the corneal epithelium of WT but not STING^{-/-} or CD118^{-/-} mice (Figure 4c). Tetherin expression was not observed in uninfected corneal epithelium (not shown). Supplemental Movie 1 highlights the differential expression of tetherin in the epithelium by 3-dimensional confocal reconstructions of WT and STING^{-/-} corneas. Punctate tetherin labeling in the deeper stromal layers of the corneas show infiltrating leukocytes which also express tetherin (Supplemental Movie 1).²⁹

Tetherin expression was also evaluated in the TG by PCR at day 5 pi (Supplemental Figure 1b) in light of evidence showing tetherin expression in neurons^{30,31} and the enhanced trafficking of HSV-1 from the cornea to the TG in STING^{-/-} and CD118^{-/-} mice observed herein (Supplemental Figure 1a). Though STING is required for tetherin expression in the corneal epithelium (Figure 4c, Supplemental Movie 1), tetherin is upregulated in the TG of STING^{-/-} mice similarly to WT at an approximate 8-fold increase over UI yet conspicuously absent in CD118^{-/-} TG at day 5 pi (Supplemental Figure 1b). The differential induction of tetherin exemplifies the specificities and complexities of IFN α / β -mediated ISG stimulation in various tissues. Furthermore, it emphasizes that and different anti-viral mechanisms control HSV-1 replication in different constituent cell types.

Tetherin impedes local HSV-1 spread and neuroinvasion

Lack of tetherin expression in the corneal epithelium of *STING*^{-/-} and *CD118*^{-/-} mice correlated with the observed increases in HSV-1 titers and unencumbered expression of HSV-1 antigen throughout the epithelium compared to WT animals. However, definitive evidence substantiating the role of tetherin in impeding local viral replication and neuroinvasion remained to be shown. siRNA transfection was used to limit tetherin expression in the corneas of WT mice pursuant to HSV-1 infection independent of ancillary IFN α / β -signaling deficiencies. Knockdown efficiency (Figure 5a) was greater than 70% at 48 hours pi at the transcript level, and trends in expression differences persisted at 72 hours pi. However, transcript expression differences were not statistically significant by the latter time point, therein demonstrating the transient nature of siRNA-mediated knockdown. Knockdown was validated at the protein level using confocal imaging to analyze the fluorescence intensity of tetherin immunolabeling in scramble and tetherin-specific siRNA-treated corneas at 72 hours pi (Figure 5b,c). Isotype control antibody labeling was used to validate the specificity of tetherin immunolabeling (Figure 5b).

Viral burden in the corneas and TG (Figure 5d) of siRNA-treated mice was subsequently measured. Local tetherin knockdown in the corneal epithelium led to a significant increase in HSV-1 titer in the cornea and TG compared to scramble siRNA transfected controls at day 3 pi (Figure 5d). Consistent with the temporary effect of tetherin knockdown, no differences in viral titer were observed by day 5 pi in the cornea or TG (not shown) comparing the two siRNA-treated groups. Collectively, our data show that tetherin is indeed a functional viral restriction factor for HSV-1 *in vivo*. Specifically, we show that tetherin expression in the corneal epithelium is *STING*-dependent. Furthermore, we demonstrate that tetherin sequesters HSV-1 in the microenvironment of the corneal epithelium in order to inhibit local cell-cell spread, impede invasion of sensory nerve fibers, and consequentially restrict viral dissemination to the nervous system.

DISCUSSION

Early IFN α / β induction through pathogen recognition receptor signaling is critical for the control of HSV-1 infection. Our previously reported data show that corneal viral titers in MyD88- or TRIF-deficient mice are no different than WT by day 5 pi;⁸ however, the corneal HSV-1 titer at day 5 pi in *STING*^{-/-} mice was more consistent with the highly susceptible *CD118*^{-/-} mice in the present study. Collectively, our data demonstrate that a TLR-independent, *STING*-dependent process mediates initial and sustained resistance to acute HSV-1 infection in the cornea prior to the induction of an adaptive immune response.

The basic resident cell composition of the murine cornea includes epithelial cells, stromal keratocytes, and endothelial cell layers in addition to tissue-resident leukocytes, sensory nerve fibers and peripheral vasculature. Each of these cell types and structures likely provide distinct contributions to defense against HSV-1 infection that collectively combat viral replication and spread. Likewise, corneal HSV-1 infection may directly or indirectly elicit unique pathologies affecting each of these components. Blood and lymphatic vessels surrounding the cornea play unique roles during infection by facilitating leukocyte influx and efflux of extracellular fluid and macromolecules, respectively.

Stark differences were observed with respect to corneal pathology comparing STING^{-/-} to CD118^{-/-} mice despite a similar viral burden. The severe corneal edema exhibited by CD118^{-/-} mice correlated with a hyperacute sensory deficit following HSV-1 infection. These findings support established notions that inflammatory processes in the cornea induce loss of innervation, and that local trophic factors maintain or restore the delicate corneal sensory fibers following injury or pathogenic insult.^{21,32,33} The present investigation expands the mechanistic understanding of corneal denervation following HSV-1 infection by identifying sensation loss transpires independent of the viral burden locally in the cornea or in the TG.

Corneal HSV-1 infection with high-titer inoculums can elicit inflammatory neovascularization during the acute stage of infection.³⁴ Moreover, lymphatic vessels are infected and destroyed by HSV-1 absence of IFN α/β signaling.²⁶ Observations from the present investigation suggest that while STING is critical for containment of HSV-1 replication and spread in the corneal epithelium, an auxiliary STING-independent yet IFN α/β -dependent pathway protects the corneal stroma and peripheral lymphatic vessels from HSV-1 infection and resultant edema.

The selective loss of mast cells in CD118^{-/-} but not in STING^{-/-} mice again supports the importance of STING-independent IFN α/β -signaling pathways in the maintenance of the corneal architecture. Mast cells likely provide support for peri-corneal lymphatic vessels and may also contribute to inflammatory lymphangiogenesis in the cornea as has been shown in other sites.³⁵⁻³⁷ Our findings collectively emphasize the importance of IFN α/β -signaling not only with respect to its anti-viral properties, but highlight its role in maintaining tissue integrity and preservation of visual acuity.

Multiple studies have established that IFN α/β signaling in both resident and bone marrow-derived cells is critical for resistance to acute HSV-1 infection in the cornea.^{23,26} We observed a profound increase in the myeloid cell infiltrate in corneas of STING^{-/-} mice relative to WT consistent with a recent report describing the role of STING-dependent suppression of excessive immune activation.³⁸ Our lab has previously shown that of the infiltrating myeloid-lineage leukocytes, inflammatory monocytes (CD45⁺ Gr-1⁺ F4/80⁺) facilitate virus clearance and are recruited by CCL2 following acute HSV-1 infection in the cornea.²³

We have now identified two distinct monocyte populations in the cornea at day 5 pi. Of these, the Ly6C⁺ Ly6G^{low} population reflects protective inflammatory monocytes. The secondary Ly6C⁺ Ly6G^{high} monocyte population observed in the cornea has been described in hypoxic metastatic niches³⁹⁻⁴¹ and during pulmonary viral infection concomitant with a lack of IFN α/β signaling and altered chemokine production.⁴² The concept of distinct monocyte subsets with notable plasticity, phenotypic variation, and functional diversity is now well established for a wide variety of pathologies.⁴³⁻⁴⁷

Inflammatory monocytes are efficiently recruited to the corneas of STING^{-/-} mice and prevent excessive tissue pathology beyond the surface barrier epithelium. *In vitro* data indicate that human macrophages and murine myeloid dendritic cells utilize a STING-

dependent pathway for recognition of HSV-1 and subsequent induction of IFN β , cytokine production, and autophagy.^{48–50} Accordingly, we investigated MHC II upregulation as an indicator of monocyte activation in the absence of STING, and found no defect compared to WT monocytes *in vitro*, though a defect in MHC II upregulation was observed in STING^{-/-} macrophages (Supplemental Figure 2c,d).

Anti-viral restriction factors serve as wardens for controlling viral infections by arresting virus replication and spread. Tetherin is a type II transmembrane protein that shares topographical homology with several prion proteins which express multiple membrane anchors, including a glycosyl-phosphatidylinositol (GPI) anchor.²⁰ Tetherin is upregulated by IFN signaling (IFN- α/β , - γ , and - λ) and is inducible in polarized epithelial cells, constitutively expressed by blood vessel endothelial cells and many leukocytes.^{18,29,51} Tetherin promotes endocytosis and degradation of enveloped virions bound to the cell surface, and is implicated in transcription of NF κ B-regulated cytokines.⁵²

Following successful replication of HSV-1 in epithelial cell nuclei, nascent HSV-1 virions must egress through the nuclear membrane, *trans*-Golgi network, and plasma membrane to infect neighboring cells.⁵³ The GPI anchor of tetherin facilitates attachment to and retention of enveloped viruses upon virion budding from the trans-Golgi network and plasma membranes to reduce cell-cell spread.⁵⁴ Furthermore, reports indicate that HSV-1 employs at least two distinct mechanisms to counteract tetherin and evade restriction *in vitro*.^{55,56} However, the *in vivo* relevance of tetherin with respect to HSV-1 infection has not been reported. Our *in vivo* data show that tetherin sequesters HSV-1 replication and spread in the cornea in addition to neurotropic spread of the virus to peripheral nerve ganglia. Furthermore, our findings detail a novel mechanism of HSV-1 restriction involving a STING-dependent, IFN α/β -mediated signaling pathway that induces tetherin on expression epithelial cells of the ocular mucosae.

METHODS

Mice and virus

C57BL/6J WT and STING^{-/-} mice were obtained from the Jackson Laboratory. CD118^{-/-} and STING^{-/-} mice were bred in-house. All mice were maintained in a specific pathogen-free vivarium at the Dean McGee Eye Institute (University of Oklahoma Health Sciences Center, Oklahoma City, OK). Mice were euthanized by cardiac perfusion with 10–15 ml of 1 \times PBS. All experimental procedures were conducted in accordance with protocols approved by Institutional Animal Care and Use Committees. HSV-1 strain McKrae was used for all experiments; the stock concentration was 7.07 \times 10⁷ plaque forming units (pfu) per ml.

Infection and plaque assays

Six to twelve week old mice were anesthetized by ketamine (100 mg/kg) and xylazine (6.6 mg/kg) injection *ip*. Following partial epithelial debridement of the cornea using a 25-gauge needle, an inoculum of 1000 pfu of HSV-1 was applied to each eye. Tissues collected from euthanized animals for standard plaque assays were homogenized and supernatants titered

on confluent CCL-81 Vero cell (ATCC, Manassas, VA) monolayers in microtiter plates as described previously.²⁸

Corneal pathology

Ultrasound pachymetry was utilized to monitor corneal thickness and edema following infection using a Corneo-Gage Plus digital pachymeter (Sonogage, Cleveland OH) as described previously.²⁸ Corneal sensation or blink reflex sensitivity was evaluated using a handheld Cochet-Bonnet esthesiometer as described previously.²¹ Cochet-Bonnet filament length-scores were interpolated into threshold sensitivity pressures using conversions provided by the manufacturer.

Gene array

Transcript expression studies on corneas were performed using PrimePCR pathway analysis technology from Bio-Rad (Hercules, CA) for selected genes according to the manufacturer's directions. RNA was isolated from corneas and converted into cDNA as described previously.⁸ Relative gene expression was calculated by the standard 2^{-Ct} method using *GAPDH* and *TBP* as reference genes following semi-quantitative real time PCR using a CFX Connect thermocycler and PrimePCR technology (Bio-Rad). Transcripts evaluated are listed in Figure 2. Gene expression profiles represented by the cluster image map in Figure 2 were generated using the National Cancer Institute's CIMminer tool freely accessible online.

Flow cytometry

Corneas were harvested from enucleated eyes of euthanized animals and digested in 2 mg/ml type 1 collagenase from *Clostridium histolyticum* (Sigma-Aldrich, St. Louis, MO) in RPMI 1640 media supplemented with 10% FBS, gentamicin, and antibiotic/antimycotic cocktail (Invitrogen, Grand Island, NY) for 2–2.5 hours at 37°C with gentle mechanical trituration every 15 minutes. The suspension was subsequently filtered through 40µm mesh, washed with 1% BSA in 1× PBS (wash buffer), pelleted, and labeled for flow cytometric analysis. Cells were immunolabeled for 30 minutes at 4°C following a 15 minute incubation with anti-CD16/32 Fc block. Antibodies were obtained from AbD Serotec (Raleigh, NC), eBioscience (San Diego, CA), BD Biosciences (San Jose, CA) to label CD11b, CD45, F4/80, I-A/I-E, Ly6C, and Ly6G leukocyte antigens. Following labeling, cells were washed twice, fixed in 1% PFA (Sigma-Aldrich) and stored overnight at 4°C. Samples were pelleted and resuspended in 1 ml wash buffer for analysis on a MacsQuant flow cytometer (Miltenyi Biotech, Bergisch Gladbach, Germany).

Immunoassays

Corneas harvested at the indicated times pi and homogenized in 1× PBS containing 1× protease inhibitor set 1 (EMD Millipore, Billerica, MA). Supernatants were used at the indicated times pi to evaluate protein concentrations of IFNα by ELISA (eBioscience) or CCL2, CCL20, IFNγ, IL-1β, and IL-17 by Bio-Plex (Biorad) suspension array according to the manufacturers' directions.

Splenocyte isolation and cultures

Spleens were harvested from euthanized mice, teased into single cell suspensions, and depleted of erythrocytes as described previously.²⁸ Immunomagnetic beads (Miltenyi Biotech) were used to isolate CD11b⁺ splenocytes by positive selection according to the manufacturer's instructions. Cultures of 1×10^5 cells were incubated at 37°C for 24–48 hours at 5% CO₂ in 1 ml RPMI 1640 media supplemented with 10% FBS, gentamicin, and antibiotic/antimycotic cocktail (Invitrogen). Supernatants were collected for plaque assay and cells were labeled for analysis by flow cytometry.

Microscopy

For confocal microscopic analysis of vasculature, mast cells, and tetherin expression, corneolimbic buttons were harvested from enucleated eyes of euthanized animals, fixed in 4% PFA for 30 minutes at 4°C, washed 3 times for 15 minutes in 1% Triton X-100 (Sigma-Aldrich) in 1× PBS, and immunolabeled or stained. Samples were washed between primary and secondary antibodies. Antibodies used to label cornea whole mounts were obtained from Abcam (Cambridge, MA), eBioscience, Dako (Carpinteria, CA), EMD Millipore, or Jackson ImmunoResearch (WestGrove, PA). FITC-conjugated avidin was used to stain peri-corneal mast cells (Biolegend, San Diego, CA) as shown previously.²⁸ Flat mounts of the tissue were prepared and imaged using an Olympus FV500 confocal microscope (Center Valley, PA). Olympus Fluoview and iMovie (Apple, Cupertino, CA) software were used to generate 3D Z-stack renderings and video highlighting the topographical localization of tetherin expression in the cornea (Supplemental Movie 1).

In vivo transfection

Ambion Silencer Select siRNA (Invitrogen) was used for corneal knockdown experiments and transfection mediated using lipofectamine 2000 (Invitrogen) as described previously.⁸ Briefly, partial epithelial debridement of corneas of anesthetized WT mice was conducted to prepare the eye for transfection. Next, 3.33 μmol tetherin-specific or nonspecific scramble control siRNA in supplement-free DMEM media was applied to each cornea in a 10 μl eye drop containing 5 μl Lipofecamine 2000 (Invitrogen). siRNA sequences were designed and validated by the manufacturer. Mice were infected with HSV-1 16 hours post-transfection. On days 2, 3, and 5 pi, tissue was harvested for plaque assay and validation of knockdown efficiency. Tetherin transcript expression was quantified using PrimePCR technology (Biorad) as described for the gene array. Tetherin protein expression was imaged in immunolabeled cornea flat mounts by confocal microscopy to evaluate knockdown efficiency.

Statistical analysis

Normal distribution of all data was assumed *a priori*. Graphical representations of data reflect mean ± SEM. Statistical analysis of all data was performed using GraphPad Prism 5 (La Jolla, CA). One- and two-way ANOVAs were used to distinguish differences among data sets while significance thresholds for sample means were identified using Student-Newman-Keuls multiple comparison tests or Bonferroni posttests, respectively. A standard unpaired Student's T test was used when applicable.

Supplementary Material

Refer to Web version on PubMed Central for supplementary material.

ACKNOWLEDGEMENTS

This work was supported by National Institutes of Health / National Eye Institute Grants R01 EY021238, P30 EY021725, and T32 EY023202. Additional support was provided by an unrestricted grant from Research to Prevent Blindness. The content of this manuscript is solely the responsibility of the authors and does not necessarily represent the official views of the NIH. The authors would like to thank Mark Dittmar and the DMEI Vivarium staff for their help in maintaining our animals; Helen Rosenberg, Ph.D. for the original source of CD118^{-/-} mice; and Meghan Carr, Jeremy Jenkins, and Min Zheng for technical assistance.

REFERENCES

1. Perry AK, Chen G, Zheng D, Tang H, Cheng G. The host type I interferon response to viral and bacterial infections. *Cell Res.* 2005; 15:407–422. [PubMed: 15987599]
2. Ivashkiv LB, Donlin LT. Regulation of type I interferon responses. *Nat. Rev. Immunol.* 2013; 14:36–49. [PubMed: 24362405]
3. Randall RE, Goodbourn S. Interferons and viruses: an interplay between induction, signalling, antiviral responses and virus countermeasures. *J. Gen. Virol.* 2008; 89:1–47. [PubMed: 18089727]
4. Duggal NK, Emerman M. Evolutionary conflicts between viruses and restriction factors shape immunity. *Nat. Rev. Immunol.* 2012; 12:687–695. [PubMed: 22976433]
5. Barber GN. Innate immune DNA sensing pathways: STING, AIMII and the regulation of interferon production and inflammatory responses. *Curr. Opin. Immunol.* 2011; 23:10–20. [PubMed: 21239155]
6. Rathinam VAK, Fitzgerald KA. Innate immune sensing of DNA viruses. *Virology.* 2011; 411:153–162. [PubMed: 21334037]
7. Wu J, Chen ZJ. Innate Immune Sensing and Signaling of Cytosolic Nucleic Acids. *Annu. Rev. Immunol.* 2014; 32:461–488. [PubMed: 24655297]
8. Conrady CD, Zheng M, Fitzgerald KA, Liu C, Carr DJJ. Resistance to HSV-1 infection in the epithelium resides with the novel innate sensor, IFI-16. *Mucosal Immunol.* 2012; 5:173–183. [PubMed: 22236996]
9. Burdette DL, Vance RE. STING and the innate immune response to nucleic acids in the cytosol. *Nat. Immunol.* 2013; 14:19–26. [PubMed: 23238760]
10. Tanaka Y, Chen ZJ. STING specifies IRF3 phosphorylation by TBK1 in the cytosolic DNA signaling pathway. *Sci. Signal.* 2012; 5:ra20. [PubMed: 22394562]
11. Unterholzner L, et al. IFI16 is an innate immune sensor for intracellular DNA. *Nat. Immunol.* 2010; 11:997–1004. [PubMed: 20890285]
12. Orzalli MH, DeLuca NA, Knipe DM. PNAS Plus: Nuclear IFI16 induction of IRF-3 signaling during herpesviral infection and degradation of IFI16 by the viral ICP0 protein. *Proc. Natl. Acad. Sci.* 2012; 109:E3008–E3017. [PubMed: 23027953]
13. Lin R, Noyce RS, Collins SE, Everett RD, Mossman KL. The herpes simplex virus ICP0 RING finger domain inhibits IRF3- and IRF7-mediated activation of interferon-stimulated genes. *J. Virol.* 2004; 78:1675–1684. [PubMed: 14747533]
14. Paladino P, Collins SE, Mossman KL. Cellular Localization of the Herpes Simplex Virus ICP0 Protein Dictates Its Ability to Block IRF3-Mediated Innate Immune Responses. *PLoS ONE.* 2010; 5:e10428. [PubMed: 20454685]
15. Royer DJ, Cohen AW, Carr DJ. The current state of vaccine development for ocular HSV-1 infection. *Expert Rev. Ophthalmol.* 2015; 10:113–126. [PubMed: 25983856]
16. Conrady CD, et al. Microglia and a Functional Type I IFN Pathway Are Required To Counter HSV-1-Driven Brain Lateral Ventricle Enlargement and Encephalitis. *J. Immunol.* 2013; 190:2807–2817. [PubMed: 23382563]

17. Bonini S, Rama P, Olzi D, Lambiase A. Neurotrophic keratitis. *Eye*. 2003; 17:989–995. [PubMed: 14631406]
18. Hotter D, Sauter D, Kirchhoff F. Emerging role of the host restriction factor tetherin in viral immune sensing. *J. Mol. Biol.* 2013; 425:4956–4964. [PubMed: 24075872]
19. Li SX, et al. Tetherin promotes the innate and adaptive cell-mediated immune response against retrovirus infection in vivo. *J. Immunol. Baltim. Md 1950.* 2014; 193:306–316.
20. Sauter D. Counteraction of the multifunctional restriction factor tetherin. *Front. Microbiol.* 2014; 5
21. Chucair-Elliott AJ, Zheng M, Carr DJJ. Degeneration and regeneration of corneal nerves in response to HSV-1 infection. *Invest. Ophthalmol. Vis. Sci.* 2015; 56:1097–1107. [PubMed: 25587055]
22. Testoni B, et al. Chromatin dynamics of gene activation and repression in response to interferon alpha (IFN α) reveal new roles for phosphorylated and unphosphorylated forms of the transcription factor STAT2. *J. Biol. Chem.* 2011; 286:20217–20227. [PubMed: 21498520]
23. Conrady CD, Zheng M, Mandal NA, van Rooijen N, Carr DJJ. IFN- α -driven CCL2 production recruits inflammatory monocytes to infection site in mice. *Mucosal Immunol.* 2013; 6:45–55. [PubMed: 22692455]
24. Shi C, Pamer EG. Monocyte recruitment during infection and inflammation. *Nat. Rev. Immunol.* 2011; 11:762–774. [PubMed: 21984070]
25. Ishikawa H, Ma Z, Barber GN. STING regulates intracellular DNA-mediated, type I interferon-dependent innate immunity. *Nature.* 2009; 461:788–792. [PubMed: 19776740]
26. Bryant-Hudson KM, et al. HSV-1 targets lymphatic vessels in the eye and draining lymph node of mice leading to edema in the absence of a functional type I interferon response. *Am. J. Pathol.* 2013; 183:1233–1242. [PubMed: 23911821]
27. Wernersson S, Pejler G. Mast cell secretory granules: armed for battle. *Nat. Rev. Immunol.* 2014; 14:478–494. [PubMed: 24903914]
28. Royer DJ, Zheng M, Conrady CD, Carr DJJ. Granulocytes in Ocular HSV-1 Infection: Opposing Roles of Mast Cells and Neutrophils. *Invest. Ophthalmol. Vis. Sci.* 2015; 56:3763–3775. [PubMed: 26066745]
29. Erikson E, et al. In vivo expression profile of the antiviral restriction factor and tumor-targeting antigen CD317/BST-2/HM1.24/tetherin in humans. *Proc. Natl. Acad. Sci. U. S. A.* 2011; 108:13688–13693. [PubMed: 21808013]
30. Sarojini S, Theofanis T, Reiss CS. Interferon-induced tetherin restricts vesicular stomatitis virus release in neurons. *DNA Cell Biol.* 2011; 30:965–974. [PubMed: 21919738]
31. Holmgren AM, Miller KD, Cavanaugh SE, Rall GF. Bone marrow stromal antigen-2 (Bst2)/tetherin is induced in neurons by type I interferon and viral infection, but is dispensable for protection against neurotropic viral challenge. *J. Virol.* 2015 JVI.01745–15.
32. Sarkar J, et al. CD11b+GR1+ myeloid cells secrete NGF and promote trigeminal ganglion neurite growth: implications for corneal nerve regeneration. *Invest. Ophthalmol. Vis. Sci.* 2013; 54:5920–5936. [PubMed: 23942970]
33. Guaiquil VH, et al. VEGF-B selectively regenerates injured peripheral neurons and restores sensory and trophic functions. *Proc. Natl. Acad. Sci. U. S. A.* 2014; 111:17272–17277. [PubMed: 25404333]
34. Wuest TR, Carr DJJ. VEGF-A expression by HSV-1-infected cells drives corneal lymphangiogenesis. *J. Exp. Med.* 2010; 207:101–115. [PubMed: 20026662]
35. Kunder CA, St John AL, Abraham SN. Mast cell modulation of the vascular and lymphatic endothelium. *Blood.* 2011; 118:5383–5393. [PubMed: 21908429]
36. Raica M, et al. Mast cells stimulate lymphangiogenesis in the gingiva of patients with periodontal disease. *Vivo Athens Greece.* 2015; 29:29–34.
37. Marone G, Varricchi G, Loffredo S, Granata F. Mast cells and basophils in inflammatory and tumor angiogenesis and lymphangiogenesis. *Eur. J. Pharmacol.* 2015
38. Sharma S, et al. Suppression of systemic autoimmunity by the innate immune adaptor STING. *Proc. Natl. Acad. Sci. U. S. A.* 2015; 112:E710–E717. [PubMed: 25646421]

39. Kowanetz M, et al. Granulocyte-colony stimulating factor promotes lung metastasis through mobilization of Ly6G+Ly6C+ granulocytes. *Proc. Natl. Acad. Sci. U. S. A.* 2010; 107:21248–21255. [PubMed: 21081700]
40. Yang XD, et al. Histamine deficiency promotes inflammation-associated carcinogenesis through reduced myeloid maturation and accumulation of CD11b+Ly6G+ immature myeloid cells. *Nat. Med.* 2011; 17:87–95. [PubMed: 21170045]
41. Sceneay J, et al. Primary tumor hypoxia recruits CD11b+/Ly6Cmed/Ly6G+ immune suppressor cells and compromises NK cell cytotoxicity in the premetastatic niche. *Cancer Res.* 2012; 72:3906–3911. [PubMed: 22751463]
42. Seo S-U, et al. Type I interferon signaling regulates Ly6C(hi) monocytes and neutrophils during acute viral pneumonia in mice. *PLoS Pathog.* 2011; 7:e1001304. [PubMed: 21383977]
43. Gordon S, Taylor PR. Monocyte and macrophage heterogeneity. *Nat. Rev. Immunol.* 2005; 5:953–964. [PubMed: 16322748]
44. Strauss-Ayali D, Conrad SM, Mosser DM. Monocyte subpopulations and their differentiation patterns during infection. *J. Leukoc. Biol.* 2007; 82:244–252. [PubMed: 17475785]
45. Rose S, Misharin A, Perlman H. A novel Ly6C/Ly6G–based strategy to analyze the mouse splenic myeloid compartment. *Cytom. Part J. Int. Soc. Anal. Cytol.* 2012; 81:343–350.
46. Mitchell AJ, Roediger B, Weninger W. Monocyte homeostasis and the plasticity of inflammatory monocytes. *Cell. Immunol.* 2014; 291:22–31. [PubMed: 24962351]
47. Xiong H, Pamer EG. Monocytes and infection: modulator, messenger and effector. *Immunobiology.* 2015; 220:210–214. [PubMed: 25214476]
48. Zhang Z, et al. The helicase DDX41 senses intracellular DNA mediated by the adaptor STING in dendritic cells. *Nat. Immunol.* 2011; 12:959–965. [PubMed: 21892174]
49. Rasmussen SB, et al. Activation of autophagy by α -herpesviruses in myeloid cells is mediated by cytoplasmic viral DNA through a mechanism dependent on stimulator of IFN genes. *J. Immunol.* 2011; 187:5268–5276. [PubMed: 21998456]
50. Horan KA, et al. Proteasomal degradation of herpes simplex virus capsids in macrophages releases DNA to the cytosol for recognition by DNA sensors. *J. Immunol.* 2013; 190:2311–2319. [PubMed: 23345332]
51. Rollason R, Korolchuk V, Hamilton C, Jepson M, Banting G. A CD317/tetherin-RICH2 complex plays a critical role in the organization of the subapical actin cytoskeleton in polarized epithelial cells. *J. Cell Biol.* 2009; 184:721–736. [PubMed: 19273615]
52. Galão RP, Le Tortorec A, Pickering S, Kueck T, Neil SJD. Innate Sensing of HIV-1 Assembly by Tetherin Induces NF κ B-Dependent Proinflammatory Responses. *Cell Host Microbe.* 2012; 12:633–644. [PubMed: 23159053]
53. Johnson DC, Wisner TW, Wright CC. Herpes Simplex Virus Glycoproteins gB and gD Function in a Redundant Fashion To Promote Secondary Envelopment. *J. Virol.* 2011; 85:4910–4926. [PubMed: 21411539]
54. Martin-Serrano J, Neil SJD. Host factors involved in retroviral budding and release. *Nat. Rev. Microbiol.* 2011; 9:519–531. [PubMed: 21677686]
55. Zenner HL, Mauricio R, Banting G, Crump CM. Herpes simplex virus 1 counteracts tetherin restriction via its virion host shutoff activity. *J. Virol.* 2013; 87:13115–13123. [PubMed: 24067977]
56. Blondeau C, et al. Tetherin restricts herpes simplex virus 1 and is antagonized by glycoprotein M. *J. Virol.* 2013; 87:13124–13133. [PubMed: 24067975]

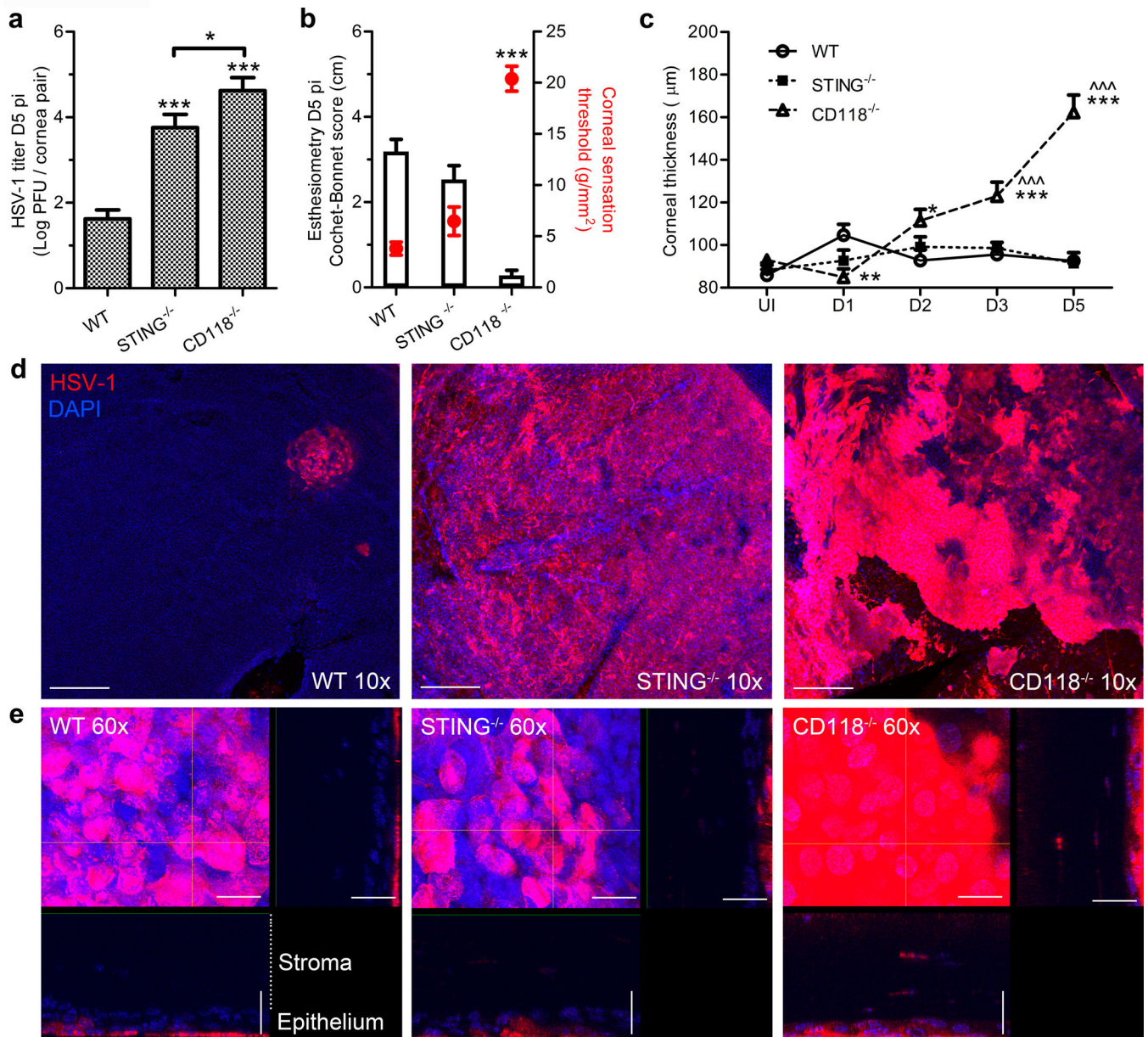


Figure 1. Viral burden and acute pathology in the cornea

(a) Viral titers at day 5 pi in fellow corneas of WT, STING^{-/-}, and CD118^{-/-} mice ($n = 7-8$ mice/group, 3 independent experiments). (b) Corneal sensitivity measured using a Cochet-Bonnet esthesiometer on day 5 pi. Black bars reflect Cochet-Bonnet score/ filament length in cm (left axis); red open circles reflect corneal sensation threshold in g/mm² (right axis), *i.e.* minimum pressure required to elicit a blink response ($n = 16$ corneas/group, 3 independent experiments). (c) Ultrasound pachymetry measurements of corneal thickness in uninfected and infected mice through day 5 pi ($n = 14-20$ corneas/group/time point; 4 independent experiments). For panel c, * indicates differences between WT and STING^{-/-} or CD118^{-/-}; ^ indicates differences between STING^{-/-} and CD118^{-/-} mice; significance threshold: * $p < 0.05$, ** $p < 0.01$, *** $p < 0.001$. (d) Representative 10× confocal images illustrating

localization of viral antigen in cornea whole mounts at day 5 pi; scale bar = 100 μm . (e) 60 \times images of viral lesions from (d) with 60 μm z-stack focal projections illustrating HSV-1 labeling in the epithelium and penetration into the stroma; scale bar = 20 μm .

Author Manuscript

Author Manuscript

Author Manuscript

Author Manuscript

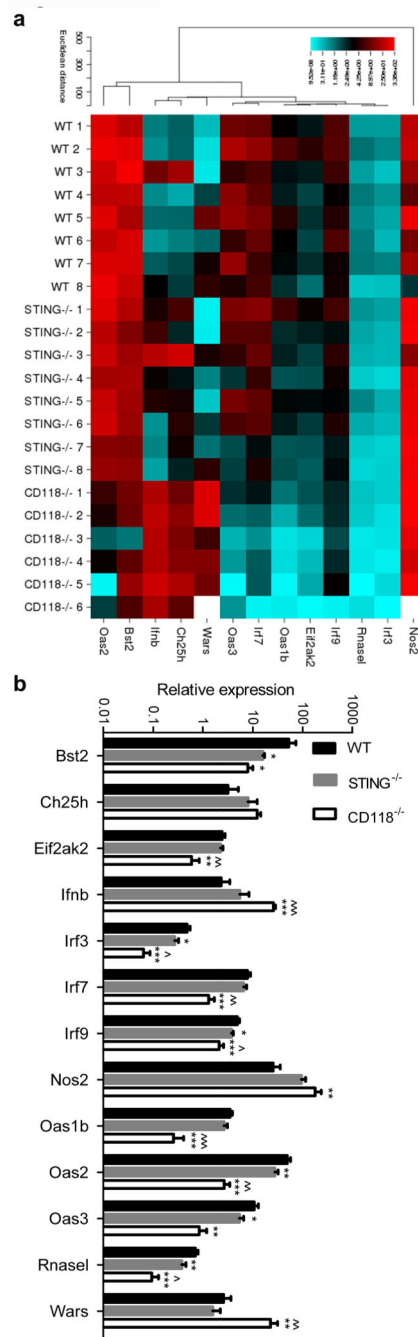


Figure 2. IFN α/β regulated gene expression

(a) Cluster image map summary of selected IFN α/β -regulated transcript expression relative to the geometric mean of GAPDH and TBP expression at day 5 pi (standardized to UI WT corneas using the 2^{-CT} method). (b) Quantified expression values for selected genes ($n = 6-8$ mice/group; 3 independent experiments). For panel b, * indicates differences between WT and STING $^{-/-}$ or CD118 $^{-/-}$; ^ indicates differences between STING $^{-/-}$ and CD118 $^{-/-}$ mice; * $p < 0.05$, ** $p < 0.01$, *** $p < 0.001$. Bst2 (Bone marrow stromal antigen 2; tetherin), Ch25h (cholesterol 25 hydroxylase), Eif2ak2 (eukaryotic initiation factor 2 α kinase 2), Ifnb

(IFN β), Irf (IFN regulatory factor), Nos2 (inducible nitric oxide synthase), Oas (oligoadenylate synthetase), Rnasel (2'-5' Oas-dependent ribonuclease), Wars (tryptophan aminoacyl-tRNA synthetase).

Author Manuscript

Author Manuscript

Author Manuscript

Author Manuscript

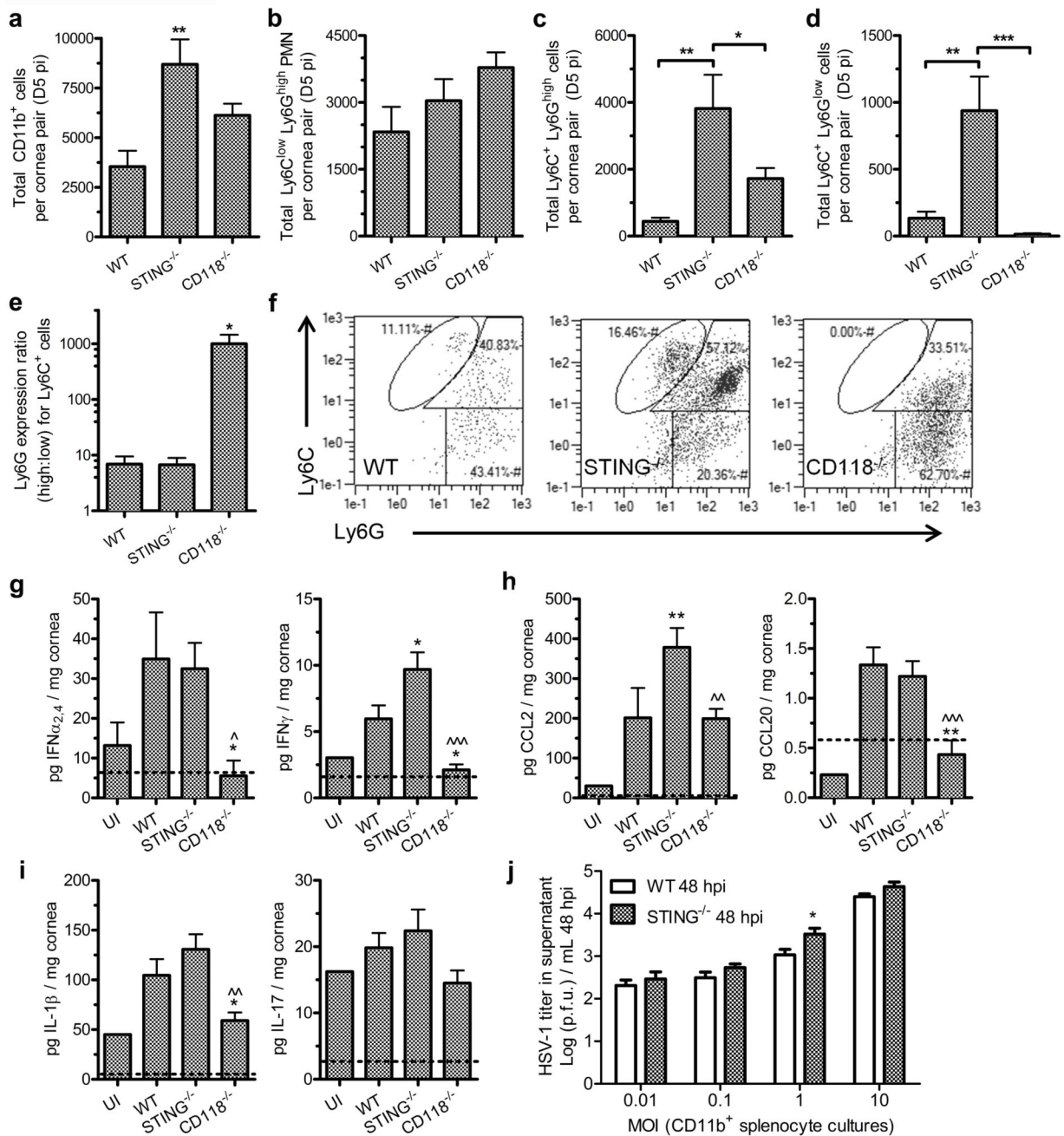


Figure 3. Leukocyte recruitment and function

Total cornea-infiltrating CD45⁺ CD11b⁺ myeloid-lineage leukocytes (a), Ly6C^{low} Ly6G^{hi} PMN (b), Ly6C⁺ Ly6G^{high} monocytes (c), Ly6C⁺ Ly6G^{low} monocytes (d) at day 5 pi (*n* = 8 mice/group; 3 independent experiments). (e) Ratio of cornea-infiltrating Ly6G^{high}:Ly6G^{low} Ly6C⁺ monocytes. (f) Representative flow plots of cornea-infiltrating CD45⁺ CD11b⁺ myeloid-lineage leukocyte subsets in WT, STING^{-/-} and CD118^{-/-} mice are featured in the following gates: Ly6C⁺ Ly6G^{low} monocytes (top central), Ly6C⁺ Ly6G^{hi} monocytes (top right), Ly6C^{low} Ly6G^{hi} PMN (lower right). Protein concentrations of IFN_{α2,4} and IFN_γ (g);

monocyte-chemotactic cytokines CCL2 (c-c motif chemokine ligand 2) and CCL20 (h); and inflammatory mediators IL-1 β and IL-17 (i) in cornea pairs at day 5 pi ($n = 10-17$ mice/group infected, 1-3 UI controls; 2-3 independent experiments). For panels (g - i), * indicates differences between WT and STING^{-/-} or CD118^{-/-}; ^ indicates differences between STING^{-/-} and CD118^{-/-} mice. (j) Viral titers from supernatants of CD11b-enriched splenocytes cultured *in vitro* with HSV-1 for 48 hours at various multiplicities of infection (MOI) ($n = 3-6$ culture samples per group; 2 independent experiments). Significance thresholds: * $p < 0.05$, ** $p < 0.01$, *** $p < 0.001$ comparing the indicated groups.

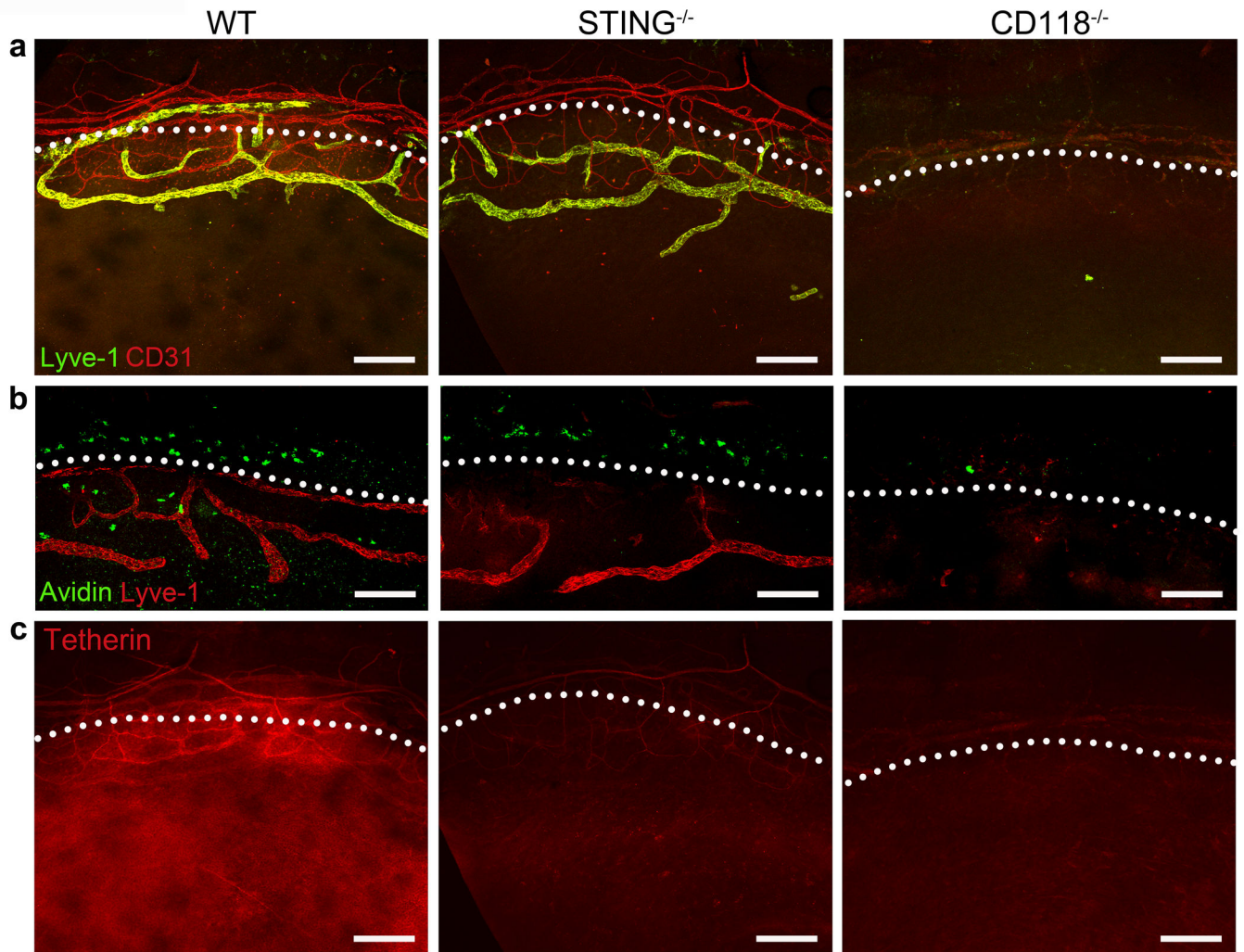


Figure 4. Vasculature, mast cells, and tetherin expression at day 5 pi

Representative 10× immunofluorescent confocal images of cornea flat mounts prepared at day 5 pi from 3–5 mice/group are shown. Lymphatic and blood vessels were labeled using Lyve-1 and CD31-specific antibodies, respectively (a). Mast cells stained with FITC-avidin reside along the limbal margin demarcated by Lyve-1 positive lymphatic vessels (b). Tetherin immunolabeling (c) highlights the constitutive tetherin expression on blood but not lymphatic vessels, and IFN-inducible expression in the epithelium (images in panels a and c are of the same sample). White dotted lines demarcate the separation between the cornea and limbus. Scale bars = 100 μm.

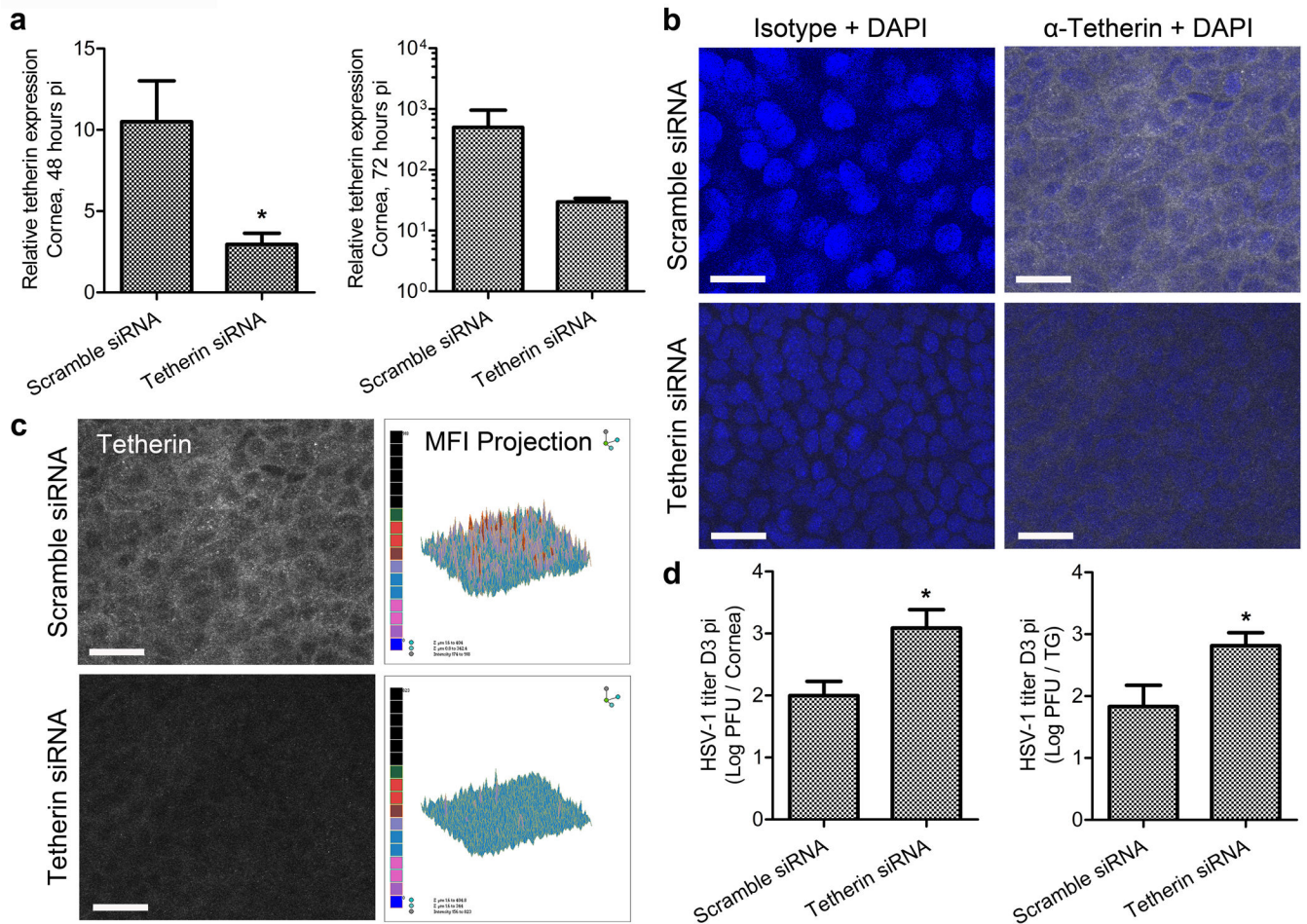


Figure 5. Tetherin restricts local HSV-1 spread and neuroinvasion *in vivo*

Corneas of WT mice were transfected with scramble or tetherin-specific siRNA, infected, animals euthanized at day 3 or 5 pi, corneas and TG harvested for PCR, 40 \times confocal imaging, or plaque assay on corneas and TG. (a) Quantification of tetherin expression relative to GAPDH and TBP expression in transfected corneas at 48 and 72 hours pi ($n = 5$ animals/group/end point; 2 independent experiments; * = p value 0.05). (b) Representative images of isotype or tetherin-specific antibody labeling with DAPI stain for contrast in the corneal epithelial layers of target or scramble siRNA transfected corneas at day 3 pi (scale bar = 20 μ m). (c) Relative siRNA-mediated tetherin protein knockdown shown as images and isometric histogram projections of tetherin MFI from panel b. Imaging was conducted on 3–4 corneas/group; 2–3 independent experiments. (d) HSV-1 titers in individual scramble control and tetherin-specific siRNA transfected mouse corneas (representative data from 1 of 2 experiments shown; $n = 6$ –7 corneas/group total) and TG ($n = 8$ –9 TG/group; 3 independent experiments); * = $p < 0.05$ comparing scramble siRNA to tetherin siRNA transfected groups.